

Correlated nature of hybrid *s*-wave superconducting and Rashba lattices

L. Craco

*Institute of Physics, Federal University of Mato Grosso, 78060-900, Cuiabá, MT, Brazil
and Leibniz Institute for Solid State and Materials Research Dresden, D-01069 Dresden, Germany* (Received 24 March 2021; revised 16 August 2021; accepted 16 August 2021; published 25 August 2021)

We elucidate the electronic state of a two-dimensional (2D) Rashba square lattice proximitized to a square monolayer *s*-wave superconductor, analyzing the role played by dynamical electron-electron interactions. The 2D+2D proximity effect induces sharp Bogoliubov and low-energy Andreev-reflected bound states, suppressing the *s*-wave gap globally. Dynamical correlations strongly renormalize the Bogoliubov quasiparticles and the Andreev levels, evolving the spin-resolved Andreev linewidths into a single bound state. We explore the channel- and spin-resolved spectral functions and analyze the reconstructed superconducting state, showing that the Rashba spin-orbit coupling drives strong channel differentiation. The mutual interplay between electron-electron and spin-orbit interactions, with proximity-induced electron pairing, lead us to introduce a generally applicable mechanism for designing Majorana fermions in 2D superconducting structures.

DOI: [10.1103/PhysRevB.104.064509](https://doi.org/10.1103/PhysRevB.104.064509)**I. INTRODUCTION**

The coupling of a superconductor (conventional *s*-wave or not) to a metal or a semiconductor results in the superconducting proximity effect in the normal system [1]. Relevant in this context is the proximity effect between superconductors and Rashba spin-split two-dimensional (2D) electron gases [2]: Due to the Rashba spin-orbit interaction a 2D electron gas shows broken inversion symmetry, manifesting itself in the so-called Rashba splitting of the electronic states [3,4]. Being proximitized to an *s*-wave superconductor, a semiconductor thin film with Rashba spin splitting may undergo a peculiar phase transition and turn into a topological superconductor [5]. Here, the states with opposite spins at opposite momenta can be paired via the proximity to an *s*-wave superconductor, which would support zero-energy Majorana fermion modes in hybrid systems [6,7]. Within the spin-orbit-coupled physics context, attention has also been given to correlated metallic and Mott insulating systems with lifted spin degeneracy, where the interplay between the Mott-Hubbard and spin-orbit interaction determines the nature of the low-energy electronic and magnetic excitations [8–11]. With this in place, in this paper we explore the interplay between electron-electron interactions, Rashba spin splitting, and *s*-wave superconductivity in a hybrid setup (see Fig. 1) composed of two correlated monolayer square lattices.

It is now recognized that a large class of systems [12–15] show coexisting symmetry-breaking phases and electron-electron correlation effects [16,17]. Particularly relevant is the discovery of materials featuring strong Rashba spin-orbit coupling and strong electronic correlations, which raises questions about the interplay of Mott and Rashba physics [9], including the emergence of superconducting (SC) phases in Rashba-Hubbard-like models [10,13,14,16,18,19]. While

the effect of spin-orbit coupling in weakly interacting electron systems is well studied by now, much less is known about the possible generic phases arising from the interplay between the spin-orbit and Coulomb interaction in correlated electron systems [8,12]. Hence, despite extensive investigations by theory and experiments, the interplay between these two effects and superconductivity still remains an open question [20]. Motivated thereby, in this paper we focus on dynamical electron-electron interactions in a Rashba-Hubbard system [9,10] hybridized with a correlated *s*-wave superconductor. Using the dynamical mean-field theory (DMFT) approximation [21,22], we analyze how these combined effects modify the correlated spectral functions of the proximitized system, and characterize distinct electronic features emerging in a half-filled 2D+2D square lattice structure.

II. MODEL AND METHOD

In this multiparticle study we investigate the two-channel electronic evolution of an extended Hubbard model under layer-dependent Rashba and *s*-wave pairing correlations represented, respectively, by the top and bottom layers in Fig. 1. Our 2D+2D system is the basic building block towards realistic heterostructures [23] or hybrid optical lattices of cold atoms [24], allowing us to control the dimensionality of different building blocks and to modulate physical parameters such as spin-orbit coupling, layer hybridization, SC gap symmetry, and many-particle electron-electron interactions. This wide tunability is expected to be a great advantage to realize novel phases of matter which might be absent in real materials.

The hybrid 2D+2D Hamiltonian studied here is $H = \sum_{\alpha} H_{\alpha} + H_d^{\text{SC}} + H_{cd}^{\text{hyb}}$, where $\alpha = c, d$ label, respectively, the

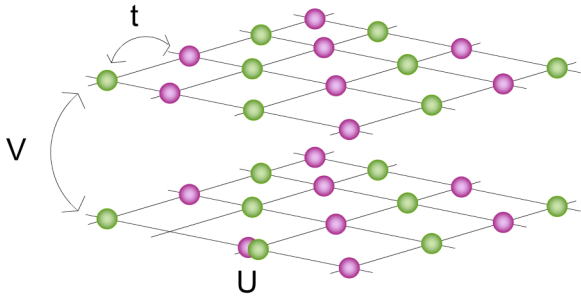


FIG. 1. Half-filled, locally hybridized bilayer lattice system. Circles represent electrons, with those of opposite spins occupying the same lattice site [24]. The arrows indicate the on-site hybridization V between the two-dimensional layers and the intralayer hopping t . In this 2D+2D layer structure all intra- and interlayer hopping elements are assumed to be equal.

Rashba spin-split and the SC square lattice, with $H_{cd}^{\text{hyb}} = V \sum_{i,\sigma} (c_{i,\sigma}^\dagger d_{i,\sigma} + \text{H.c.})$ being the local Anderson-like hybridization term [25,26] between lattices c and d . In order to keep our discussion general, and similar to Ref. [27], we will make minimal assumptions on the SC state, and consider the Rashba-Hubbard lattice in proximity with an s -wave superconductor (respectively, the top and bottom layers in Fig. 1), where the intraband interaction in the SC channel reads $H_d^{\text{SC}} = \Delta \sum_{\mathbf{k}} (d_{\mathbf{k},\uparrow}^\dagger d_{-\mathbf{k},\downarrow}^\dagger + \text{H.c.})$, with Δ being the s -wave pairing potential [26,28,29]. Moreover, consistent with earlier studies [9,10,24,30] we write the normal one-band and electron correlation terms as $H_\alpha = \sum_{\mathbf{k},\sigma} \varepsilon_\alpha(\mathbf{k}) n_{\alpha,\mathbf{k},\sigma} + U \sum_i n_{\alpha,i,\uparrow} n_{\alpha,i,\downarrow} + U' \sum_{(ij)} n_{\alpha,i} n_{\alpha,j}$, where U (U') is the on-site (intersite) [30] Coulomb interaction, and $\varepsilon_\alpha(\mathbf{k})$ are the two-channel band dispersions, which encode details of the 2D structures [9,10,24].

In a square lattice with nearest-neighbor hopping t and Rashba spin-orbit coupling t_{SO} , the one-band dispersions can be written as [9,10] $\varepsilon_d(\mathbf{k}) = \varepsilon_0(\mathbf{k})$ and $\varepsilon_c(\mathbf{k}) = \varepsilon_0(\mathbf{k}) + \gamma t_{\text{SO}} \sqrt{\sin^2(k_x) + \sin^2(k_y)}$, with $\varepsilon_0(\mathbf{k}) = -t[\cos(k_x) + \cos(k_y)]$. Here, the index $\gamma = \pm 1$ indicates the helicity [9,10] of the helical bands. These 2D band structures are the one-particle inputs for correlated electronic structure calculations within DMFT [31]. As shown below, the two-fluid assumption made here, where one fluid is an intrinsic SC and the other is a proximity-induced superconductor, has profound effects in the low-energy excitation spectrum of a hybrid system with coexisting s -wave SC and electronic states with lifted spectral degeneracy.

We evaluate the many-particle Green's functions $G_{\alpha,\sigma}(\omega, \mathbf{k}) = \frac{1}{\omega - \Sigma_{\alpha,\sigma}(\omega) - \varepsilon_\alpha(\mathbf{k})}$ of our two-channel Hamiltonian at zero temperature and real frequencies using the one-band iterated perturbation theory (IPT) impurity solver for DMFT. The detailed formulation of IPT for correlated electron systems at arbitrary fillings has already been described [32] and used in the context of extended Hubbard and periodic Anderson models [25,33] so we do not repeat the equations here. Moreover, as in earlier works, we decouple the intersite Coulomb correlation term in the Hartree approximation [34], which is exact within DMFT [31].

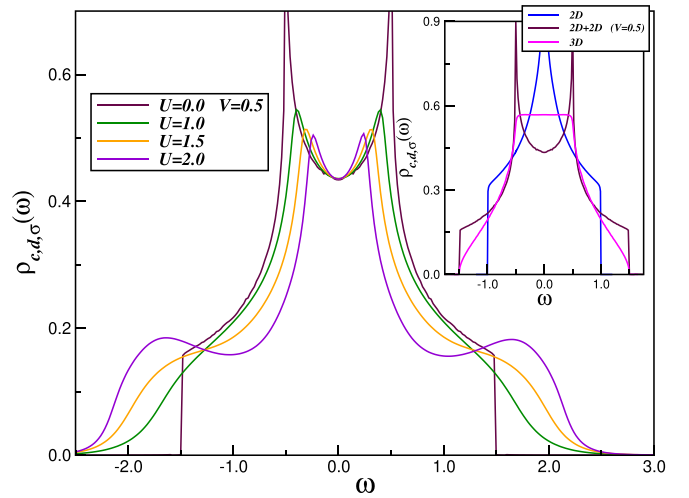


FIG. 2. Local density of states (LDOS) for the hybrid ($V = 0.5$) 2D+2D Hubbard model in the paramagnetic (non-spin-split) phase at half filling. Notice the emergent Hubbard bands with increasing the on-site Coulomb interaction U , and the zero frequency pinning of the LDOS to the bare ($U = 0.0$) value. The inset shows for comparison the bare two- (2D) and three-dimensional (3D) LDOS with the hybrid 2D+2D case.

III. RESULTS

A. Role of hybridization and Coulomb interaction

To begin with we consider the hybrid 2D+2D many-body Hamiltonian H within the $\Delta = t_{\text{SO}} = 0.0$ limit. In Fig. 2 we show the correlated electronic behavior which emerges in the local density of states (LDOS) [$\rho_{\alpha,\sigma}(\omega) = -\frac{1}{\pi} \text{Im} \sum_{\mathbf{k}} G_{\alpha,\sigma}(\omega, \mathbf{k})$] upon consideration of dynamical electron-electron interactions in our planar 2D+2D system. For the sake of simplicity we use fixed $t = V = 0.5$ and $U' = \frac{U}{2}$ values [35]. The former implies equal nearest-neighbor and interlayer hopping elements [36]. With this parameter choice the hybrid structure lies in between the true 2D and three-dimensional (3D) electron gas system, displaying the same bare one-particle bandwidth as in the 3D case (see the inset of Fig. 2). As shown in the inset of Fig. 2, due to a sizable hybridization effect the van Hove singularity of the 2D square lattice [21] splits into two [36,37], and their energies coincide with those where the 3D LDOS achieves its highest value. Remarkable as well are the changes in the LDOS with increasing the on-site Coulomb interaction U . Our results in the main panel of Fig. 2 correctly reproduce the expected behavior for the correlated spectral functions within the DMFT approximation. Particularly interesting in this context are the emergent lower (LHB) and upper (UHB) Hubbard bands, the crossing points at energies close to ± 1.3 , and the pinning of the correlated spectral function to its bare value at the Fermi energy ($E_F = \omega = 0.0$) [21,31], implying a regular Fermi liquid electronic behavior [21] in this correlated 2D+2D system.

As shown in the main panel of Fig. 2, here we numerically investigate, using the DMFT method, a simple realization of a two-layer Hubbard model in which the tunneling between layers V is equal to the single-particle hopping t . As visible in the inset of Fig. 2, this model interpolates between the

3D and 2D systems. Similar to Ref. [38], our proposal aims to overcome the limitation of searching for suitable combinations of crystal geometries, with inherent lattice-matched symmetries, to describe the electronic reconstruction in a hybrid Rashba-Hubbard *s*-wave SC system. As a starting point towards future studies, the present DMFT study is free from any particular crystal geometry, and thus provides an interesting playground for engineering heterostructures with distinct normal state properties. Another advantage of the present case (see our results below) as compared to other studies showing the formation of a Majorana corner [39] or edge states [27] is that here the Majorana zero modes emerge at each lattice site, and thus are intrinsically not isolated from bulk states.

B. Effect of multiparticle interactions and *s*-wave pairing

Aiming to shine light on the changes induced by Rashba spin-split and Coulomb interaction effects in the excitation spectrum within the SC state, we have extended our normal state electronic structure calculation to treat H_d^{MF} above within DMFT formalism for the SC state [29]. Using our assumption for the *s*-wave SC pair field Δ the DMFT equations are readily extendable to the SC regime. In this regime the Green's functions have normal and anomalous components [40,41], yielding renormalized normal $G_{\alpha,\sigma}(\omega, \mathbf{k})$ and anomalous $F_{d,\sigma}(\omega, \mathbf{k}) = G_{d,\sigma}(\omega, \mathbf{k}) \frac{\Delta}{\omega + \Sigma_{d,\sigma}^*(\omega) + \varepsilon_d(\mathbf{k})}$ propagators [42]. The former is solved by extending the normal state DMFT treatment to include an explicit pair potential term. Including the pair field Δ along with the interlayer hybridization V , the DMFT propagators are written as

$$G_{d,\sigma}(\omega, \mathbf{k}) = \frac{1}{\omega - \Sigma_{d,\sigma}(\omega) - \varepsilon_d(\mathbf{k}) - \xi_{d,\sigma}(\omega, \mathbf{k})},$$

and

$$G_{c,\sigma}(\omega, \mathbf{k}) = \frac{1}{\omega - \Sigma_{c,\sigma}(\omega) - \varepsilon_c(\mathbf{k}) - \xi_{c,\sigma}(\omega, \mathbf{k})},$$

where

$$\xi_{d,\sigma}(\omega, \mathbf{k}) = \frac{\Delta^2}{\omega + \Sigma_{d,\sigma}^*(\omega) + \varepsilon_d(\mathbf{k})} + \frac{V^2}{\omega - \Sigma_{c,\sigma}(\omega) - \varepsilon_c(\mathbf{k})},$$

and

$$\xi_{c,\sigma}(\omega, \mathbf{k}) = \frac{V^2}{\omega - \Sigma_{d,\sigma}(\omega) - \varepsilon_d(\mathbf{k}) - \frac{\Delta^2}{\omega + \Sigma_{d,\sigma}^*(\omega) + \varepsilon_d(\mathbf{k})}}.$$

As shown below, since these propagators are coupled via the interlayer hybridization V , the emergence of a SC state in the *d* band will induce remarkable SC fingerprints in the proximitized *c* shell.

In order to understand how the different channels behave regarding the SC proximity effect, we display in Fig. 3 the channel-resolved spectral functions in the absence of the Rashba spin-orbit interaction. As seen in the upper left-hand inset of Fig. 3, in the zero hybrid interlayer limit the *d* channel is strongly reshaped by the *s*-wave pairing mechanism. The clear appearance of an *s*-wave superconductor with a gapped spectrum [28,43] followed by sharp singularities at low energies is seen for $\Delta = 0.1$ in the clean 2D limit. It is worth mentioning that the appearance of sharp singularities at low energies as in Fig. 3, the so-called Bogoliubov

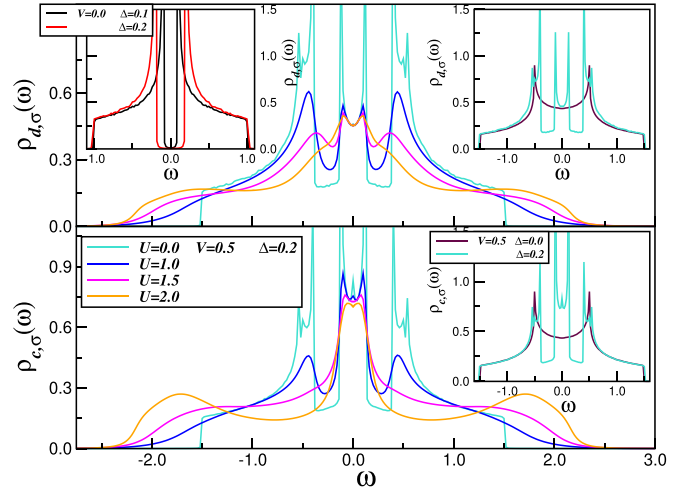


FIG. 3. Evolution of the two-channel spectral functions across the superconducting (SC) transition in the absence of Rashba spin splitting. The upper left-hand inset displays the *d*-channel LDOS for two pair-field values, showing conventional Bogoliubov quasiparticles above the *s*-wave SC gap. The upper right-hand inset shows the changes in the bare 2D+2D LDOS across the SC transition and the emergence of sharp Andreev bound states in the true *d*- and the proximitized *c*-channel superconductor. The main panels display the changes in the SC spectral functions with increasing U , showing how Bogoliubov- and Andreev-level linewidths are reshaped by local dynamical correlations.

quasiparticles, is the one-particle fingerprint of conventional *s*-wave superconductors [28]. Remarkable, however, are our results for $V = 0.5$ and $\Delta = 0.2$ in the upper right-hand inset of Fig. 3, suggesting the emergence of a topological transition within the bare SC state. Due to the proximity effect this state is marked by a closure of the SC gap, and the appearance of two low-energy modes symmetrically located around E_F . The latter suggests the emergence of Andreev-like bound states, with electrons traveling the normal (non-SC) system being Andreev reflected from the layer superconductor [6,43–45]. Moreover, due to the sizable proximity effect, superconductivity with similar reflected Andreev bound states is also induced in the *c* layer (see the lower right-hand inset of Fig. 3). Additionally, in the main panels of Fig. 3 we display the channel-selective evolution of the correlated SC state. From our results, it is evident that the Bogoliubov quasiparticles are strongly suppressed upon increasing the on-site Coulomb interactions U , with a concomitant appearance of LHBS and UHBs at high energies. Interesting as well is the evolution of the Andreev levels, which is found to be channel selective with those at the *c* channel being more stable against dynamical electron-electron interactions. Taken together, our results in the main panels of Fig. 3 suggest that the Bogoliubov- and Andreev-level linewidths are strongly reshaped by dynamical correlation effects and only SC kinks [40] are expected to be seen in spectroscopy and tunneling experiments on similar planar systems treated beyond the Hartree-Fock approximation [36].

It should be noted here that in the absence of disorder or proximity to quantum criticality, a correlated Fermi sea can be described in terms of well-defined, coherent Fermi liquid

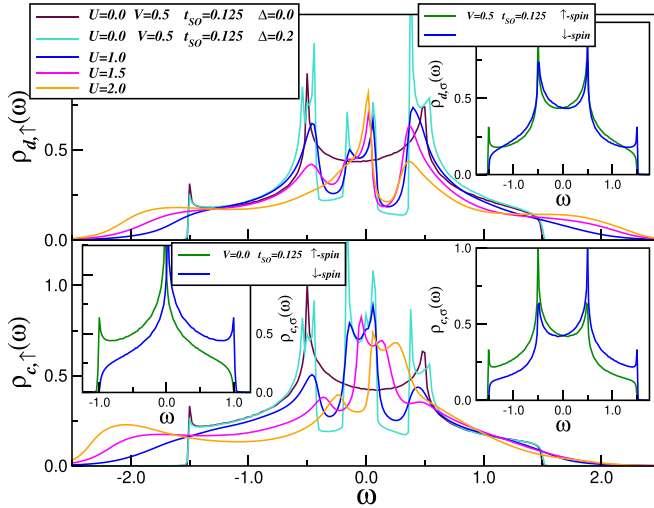


FIG. 4. 2D+2D spin-resolved spectral functions in the presence of Rashba spin splitting. The lower left-hand inset displays the 2D LDOS with lifted spectral degeneracy for fixed spin-orbit coupling (t_{SO}), showing particle-hole asymmetry and the emergence of van Hove singularities at the band edges. The right-hand insets display the combined effect of 2D+2D hybridization and spin-orbit coupling, showing less pronounced spin splitting within the bare d channel. The main panels reveal the changes in the SC spectral functions with increasing U , showing how the spin-resolved Andreev levels in the d channel evolve towards a single peak. (The \uparrow -spin normal state LDOS are also shown for comparison in the main panels).

quasiparticles at low energies as in Fig. 2. Having in mind that in DMFT the self-energy is momentum independent, the quasiparticle residue Z [31], which also defines the renormalized Fermi energies, characterizes the degree of electronic correlations of the normal metallic state, establishing the energy above which the lifetime of quasiparticles becomes short and many-particle coherence is lost. In the case of conventional s -wave superconductors the coherent length is set by the energy window of the Bogoliubov quasiparticles above the s -wave SC gap. However, due to the proximity effect in the hybrid 2D+2D system, this energy scale is further reduced to an energy window defined by the Andreev level bound states. Thus, from our results in Fig. 3, we conclude that in our 2D+2D setup the coherence length of the proximitized SC state is nearly similar to the normal state, since both are bounded by the Andreev bound states.

In Fig. 4 we show the effect of Rashba spin splitting in our hybrid 2D+2D system. To understand this, in the lower left-hand panel we consider the spin-resolved LDOS for $t_{SO} = 0.125$ [18,28,46] within the nonhybrid limit. As seen, the 2D spectral degeneracy is lifted, with a concomitant appearance of von Hove singularities at the band edges. Spin-dependent particle-hole asymmetry is also visible within the hybrid 2D+2D bare case (see the right-hand insets of Fig. 4), which as expected is more pronounced in the Rashba c channel. Moreover, due to half-filling particle-hole symmetry in the main panels of Fig. 4 we show only the evolution of the multiparticle spectra for the majority spin- \uparrow ($\gamma = -1$) sector. In spite of a clear spectral function differentiation, in both

channels the crossing points are visible at high energies with the LHBs being more pronounced as compared to the UHBs. Although upon increasing U the c channel develops a pseudo-SC gap with the Andreev levels being transferred towards the conduction band, the nearly symmetric d -band Andreev bound states turn into a zero-energy mode approaching E_F and almost cross it at $U = 2$. It should be noted that a similar spin-resolved Andreev level evolution has been observed in tunneling (dI/dV) spectra of hybrid nanostructures [45], revealing that the spin-split Andreev level crossing E_F results in a quantum phase transition to a spin-polarized state with changes in the fermionic parity of the system.

C. Emergence of Majorana zero modes

Let us now discuss the implications of our results for the emergence of Majorana modes in our hybrid bilayer setup. From the theoretical standpoint, a similar zero-energy crossing of the Andreev level as in the d channel of Fig. 4 has been reported in Refs. [45,47]. Importantly, according to Ref. [45], such zero-energy crossing manifests itself as a zero-bias conductance anomaly with properties that resemble those expected for the emergence of the Majorana modes from the Andreev bound states. Our results for $U = 1.0$ in the upper panel of Fig. 4 are also consistent with spin-polarized Majorana zero modes observed in the dI/dV spectra of magnetic Fe clusters on Bi(111) thin films grown in a SC Nb substrate [48], providing support for creating Majorana zero modes in correlated electron systems [27]. Although this resemblance is found here without evoking topological superconductivity [4], the zero-energy mode at E_F offers an electron-correlated platform to realize and manipulate many-body Majorana zero modes [49–51] in the hybrid 2D+2D limit.

To understand the changes in the electronic state which might give rise to channel-selective Majorana bound states, we show in Fig. 5 the total spectral functions $\rho_{\alpha}(\omega) = \sum_{\sigma} \rho_{\alpha,\sigma}(\omega)$ for $U = 2.0$ (main panels) and $U = 1.5$ (right insets). This is motivated by the fact that the Majorana particles are their own antiparticles [52], implying that the spectral weight of localized modes should be built on an equal footing from coherent scattering between the electron and hole components [27] as described above. As seen in Fig. 5, while the c -channel Hubbard bands are sensitive to changes in the Rashba spin-orbit interaction due to Rashba-assisted dynamical spectral weight transfer, the high in energy spectra of the SC d channel is almost insensitive to changes in t_{SO} . However, the electronic reconstruction of the d channel at lower energies is found to be surprisingly dependent on t_{SO} . From our results in the upper panel of Fig. 5, it is visible that the zero-energy mode of the normal [$\rho_d(\omega)$] and anomalous [$F_d(\omega)$] DMFT components is enhanced by the combined effects of multiparticle interactions and s -wave pairing symmetry, suggesting that the emergent Majorana modes are stable excitations in correlated s -wave superconductors locally proximitized to Rashba-Hubbard lattices.

From our results in Figs. 4 and 5, it is evident the many competing energy scales induced by multiparticle correlation effects present in our hybrid 2D+2D system lead to an emergent phenomenon for designing Majorana zero modes at low energies. Differently from the other proposed

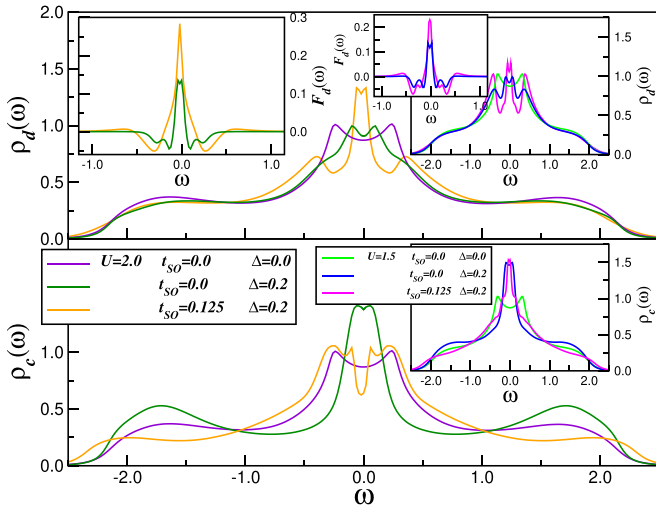


FIG. 5. Evolution of the total LDOS across the SC transition for $U = 2.0$ (main panels) [$U = 1.5$ (insets)] and two t_{SO} values. Notice the enhancement of the single Andreev peak for $t_{SO} = 0.125$ as compared to the Rashba free case within the normal [$\rho_d(\omega)$] SC component, inducing a sharp low-energy line shape in the anomalous [$F_d(\omega)$] component of the d -channel spectral functions. Also noteworthy is the t_{SO} dependence of the c channel.

candidate setups [24,36], our scheme does not require real space spin correlations [24] or Kondo exchange coupling [36]. All ingredients needed for the emergence Majorana fermions appear as a consequence of collective multiparticle quantum correlations induced by proximity and Coulomb interaction effects. Notwithstanding, apart from the cold atoms [24,53] and the heterostructure [23,54] perspectives, there are only a few candidate systems [38,45,47,48] that may exhibit the behavior found here due to their intrinsic multiband and multi-orbital quantum nature. Nonetheless, promising alternative approaches to realize Majorana fermions are thin films of iridium [55] covered by conventional BCS superconductors or chains of magnetic atoms on the surface of an s -wave superconductor [56]. Finally, due to sizable bulk quantum correlations in Bi_2Se_3 topological insulators [57], an additional efficient route for designing Majorana zero modes would be to make use of ultrafast optical excitation and manipulate the Rashba-induced spin splitting of a two-dimensional electron

gas [58] engineered at the surface of Cu-doped Bi_2Se_3 superconductor [59].

IV. CONCLUSION

In summary, in this paper we explore the physical properties of a two-dimensional Rashba-Hubbard lattice hybridized with a correlated s -wave superconductor. Our setup allows spin degeneracy to be lifted without destroying superconductivity, and suggests that the spin-split Andreev level linewidth crossing the Fermi energy results in an electronic state which changes the fermionic parity due to strong electron-electron interactions. We show how the resulting zero-energy line shape of the normal and anomalous superconducting components increase with increasing the Rashba spin-orbit interaction. This manifests itself as a low-energy anomaly with properties that resemble those expected for the emergence of many-body Majorana modes in topological superconductors [45,46,49,50]. Although the emergent low-energy mode is understood without evoking topological superconductivity [60], the resulting anomalous proximity effect is important for the ongoing discussion on the mechanisms for designing Majorana fermions [53] in correlated quantum gases [61].

Our work highlights the role of dynamical electronic correlations for understanding the emergence of an exotic electronic state which might host Majorana bound states in hybrid s -wave superconducting/Rashba-Hubbard two-dimensional lattices. Our approach can be expanded to cover other lattice systems and heterostructures to facilitate the prediction of material properties in accord with their device-level implementations. A natural extension to the study presented here is to generalize the model and method to include multi-orbital degrees of freedom. However, the extension to multi-orbital physics, especially for real materials, must take into account various processes that arise from band structures, interorbital Coulomb interactions, and Hund's coupling. Nevertheless, we expect that our present results will stimulate future studies in this direction, and ultimately complement the ongoing research efforts to devise novel routes for creating Majorana zero modes.

ACKNOWLEDGMENTS

This work is supported by CNPq (Grant No. 304035/2017-3). Acknowledgement is also made to CAPES.

- [1] C. W. J. Beenakker, *Phys. Rev. B* **46**, 12841 (1992).
- [2] See, for example, Z. H. Yang, J. Wang, and K. S. Chan, *Supercond. Sci. Technol.* **22**, 055012 (2009); C. Reeg, D. Loss, and J. Klinovaja, *Beilstein J. Nanotechnol.* **9**, 1263 (2018); S. Tamura and Y. Tanaka, *Phys. Rev. B* **99**, 184501 (2019).
- [3] Y. A. Bychkov and E. I. Rashba, *JETP Lett.* **39**, 78 (1984).
- [4] For a review article, see A. Manchon, H. C. Koo, J. Nitta, S. M. Frolov, and R. A. Duine, *Nat. Mater.* **14**, 871 (2015).
- [5] J. D. Sau, R. M. Lutchyn, S. Tewari, and S. Das Sarma, *Phys. Rev. Lett.* **104**, 040502 (2010).
- [6] E. Prada, P. San-Jose, M. W. A. de Moor, A. Geresdi, E. J. H. Lee, J. Klinovaja, D. Loss, J. Nygård, R. Aguado, and L. P. Kouwenhoven, *Nat. Rev. Phys.* **2**, 575 (2020).
- [7] B. Li, J.-B. Fu, G.-Y. Huang, and M.-T. Deng, *arXiv:2009.10985*.
- [8] J. Radić, A. Di Ciolo, K. Sun, and V. Galitski, *Phys. Rev. Lett.* **109**, 085303 (2012); W. S. Cole, S. Zhang, A. Paramekanti, and N. Trivedi, *ibid.* **109**, 085302 (2012).
- [9] V. Brosco and M. Capone, *Phys. Rev. B* **101**, 235149 (2020).
- [10] S. Wolf and S. Rachel, *Phys. Rev. B* **102**, 174512 (2020).
- [11] M. F. López and J. Merino, *Phys. Rev. B* **102**, 035157 (2020).

- [12] W. Witzczak-Krempa, G. Chen, Y. B. Kim, and L. Balents, *Annu. Rev. Condens. Matter Phys.* **5**, 57 (2014).
- [13] C. González-Ruano, L. G. Johnsen, D. Caso, C. Tiusan, M. Hehn, N. Banerjee, J. Linder, and F. G. Aliev, *Phys. Rev. B* **102**, 020405(R) (2020).
- [14] K. Nogaki and Y. Yanase, *Phys. Rev. B* **102**, 165114 (2020).
- [15] D. Bercioux and P. Lucignano, *Rep. Prog. Phys.* **78**, 106001 (2015); A. Riefer, M. Friedrich, S. Sanna, U. Gerstmann, Arno Schindlmayr, and W. G. Schmidt, *Phys. Rev. B* **93**, 075205 (2016); X. Cai, Y. Ayino, J. Yue, P. Xu, B. Jalan, and V. S. Pribiag, *ibid.* **100**, 081402(R) (2019); T. S. Suraj, G. J. Omar, H. Jani, M. M. Juvaid, S. Hooda, A. Chaudhuri, A. Rusydi, K. Sethupathi, T. Venkatesan, A. Ariando, and M. S. Ramachandra Rao, *ibid.* **102**, 125145 (2020).
- [16] R. Ghadimi, M. Kargarian, and S. A. Jafari, *Phys. Rev. B* **99**, 115122 (2019).
- [17] See, for example, M. Hohenadler, and F. F. Assaad, *Phys. Rev. B* **90**, 245148 (2014); V. Brosco, D. Guerci, and M. Capone, *ibid.* **97**, 125103 (2018); L.-D. Zhang, X. Zhang, J.-J. Hao, W. Huang, and F. Yang, *ibid.* **99**, 094511 (2019), and references therein.
- [18] A. Greco and A. P. Schnyder, *Phys. Rev. Lett.* **120**, 177002 (2018).
- [19] X. Lu and D. Sénéchal, *Phys. Rev. B* **98**, 245118 (2018).
- [20] K. Li, *Phys. Rev. B* **102**, 165150 (2020).
- [21] R. Žitko, J. Bonča, and T. Pruschke, *Phys. Rev. B* **80**, 245112 (2009).
- [22] H. Zenia, J. K. Freericks, H. R. Krishnamurthy, and Th. Pruschke, *Phys. Rev. Lett.* **103**, 116402 (2009); see also A. Vranić, J. Vučićević, J. Kokalj, J. Skolimowski, R. Žitko, J. Mravlje, D. Tanasković, *Phys. Rev. B* **102**, 115142 (2020).
- [23] K. Nakayama, S. Souma, C. X. Trang, D. Takane, C. Chen, J. Avila, T. Takahashi, S. Sasaki, K. Segawa, M. C. Asensio, Y. Ando, and T. Sato, *Nano Lett.* **19**, 3737 (2019).
- [24] E. Ibarra-García-Padilla, R. Mukherjee, R. G. Hulet, K. R. A. Hazzard, T. Paiva, and R. T. Scalettar, *Phys. Rev. A* **102**, 033340 (2020).
- [25] L. Craco, *J. Phys.: Condens. Matter* **11**, 8689 (1999); *Phys. Rev. B* **77**, 125122 (2008).
- [26] R. Žitko, J. S. Lim, R. López, and R. Aguado, *Phys. Rev. B* **91**, 045441 (2015).
- [27] J. Herbrych, M. Środa, G. Alvarez, M. Mierzejewski, and E. Dagotto, *Nat. Commun.* **12**, 2955 (2021).
- [28] N. F. Q. Yuan and L. Fu, *Phys. Rev. B* **97**, 115139 (2018).
- [29] L. Craco, M. S. Laad, and S. Leoni, *Sci. Rep.* **7**, 2632 (2017).
- [30] L. Craco, M. S. Laad, S. Leoni, and H. Rosner, *Phys. Rev. B* **79**, 075125 (2009).
- [31] A. Georges, G. Kotliar, W. Krauth, and M. J. Rozenberg, *Rev. Mod. Phys.* **68**, 13 (1996).
- [32] H. Kajueter and G. Kotliar, *Phys. Rev. Lett.* **77**, 131 (1996).
- [33] M. S. Laad, L. Craco, and E. Müller-Hartmann, *Phys. Rev. B* **64**, 195114 (2001).
- [34] L. Craco, M. S. Laad, and E. Müller-Hartmann, *Phys. Rev. B* **74**, 064425 (2006); L. Craco, M. S. Laad, S. Leoni, and A. S. de Arruda, *ibid.* **87**, 155109 (2013).
- [35] Here, all model parameters and energy scales are in units of $\tilde{W} = 2t = 1$, i.e., the half bandwidth of the bare 2D lattice.
- [36] S. dos Anjos Sousa-Júnior, J. P. de Lima, N. C. Costa, and R. R. dos Santos, *Phys. Rev. Research* **2**, 033168 (2020).
- [37] M. Golor, T. Reckling, L. Classen, M. M. Scherer, and S. Wessel, *Phys. Rev. B* **90**, 195131 (2014).
- [38] T. Das and A. V. Balatsky, *Nat. Commun.* **4**, 1972 (2013).
- [39] Y.-X. Li and T. Zhou, *Phys. Rev. B* **103**, 024517 (2021).
- [40] M. S. Laad and L. Craco, *Phys. Rev. Lett.* **103**, 017002 (2009).
- [41] M. A. Sulangi and J. Zaanen, *Phys. Rev. B* **98**, 094518 (2018).
- [42] The * denotes complex conjugation.
- [43] A. Das, Y. Ronen, Y. Most, Y. Oreg, M. Heiblum, and H. Shtrikman, *Nat. Phys.* **8**, 887 (2012).
- [44] See J. A. Sauls, *Philos. Trans. R. Soc., A* **376**, 2125 (2018); see also T. Elalaily, O. Kürtössy, V. Zannier, Z. Scherübl, I. E. Lukács, P. Srivastava, F. Rossi, L. Sorba, S. Csonka, and P. Makk, *Phys. Rev. Applied* **14**, 044002 (2020); C. Jünger, A. Baumgartner, R. Delagrangé, D. Chevallier, S. Lehmann, M. Nilsson, K. A. Dick, C. Thelander, and C. Schönenberger, *Commun. Phys.* **2**, 76 (2019), and references therein.
- [45] E. J. H. Lee, X. Jiang, M. Houzet, R. Aguado, C. M. Lieber, and S. De Franceschi, *Nat. Nanotechnol.* **9**, 79 (2014).
- [46] S. B. Chung, C. Chan, and H. Yao, *Sci. Rep.* **6**, 25184 (2016).
- [47] G. Górski, J. Barański, I. Weymann, and T. Domański, *Sci. Rep.* **8**, 15717 (2018).
- [48] B. Jäck, Y. Xie, J. Li, S. Jeon, B. A. Bernevig, and A. Yazdani, *Science* **364**, 1255 (2020).
- [49] H.-H. Hung, J. Wu, K. Sun, and C.-K. Chiu, *Sci. Rep.* **7**, 3499 (2017).
- [50] I. J. van Beek and B. Braunecker, *Phys. Rev. B* **94**, 115416 (2016).
- [51] J. D. Cifuentes and L. G. G. V. Dias da Silva, *Phys. Rev. B* **100**, 085429 (2019).
- [52] S. R. Elliott and M. Franz, *Rev. Mod. Phys.* **87**, 137 (2015).
- [53] X.-S. Ye, Y. J. Liu, X. Y. Zhang, and G. Wu, *Sci. Rep.* **7**, 13541 (2017).
- [54] R. M. Lutchyn, E. P. A. M. Bakkers, L. P. Kouwenhoven, P. Krogstrup, C. M. Marcus, and Y. Oreg, *Nat. Rev. Mater.* **3**, 52 (2018).
- [55] U. Nagel, A. Nowak, E. Kellner, H.-J. Gebauer, P. Colling, S. Cooper, D. Dummer, P. Ferger, M. Frank, P. Freund, G. Forster, J. Igalson, A. Nucciotti, F. Pröbst, A. Rulofs, W. Seidel, and L. Stodlsky, *J. Low Temp. Phys.* **93**, 543 (1993).
- [56] S. Nadj-Perge, I. K. Drozdov, B. A. Bernevig, and A. Yazdani, *Phys. Rev. B* **88**, 020407(R) (2013).
- [57] L. Craco and S. Leoni, *Phys. Rev. B* **85**, 075114 (2012).
- [58] M. Michiardi, F. Boschini, H.-H. Kung, M. X. Na, S. K. Y. Dufresne, A. Currie, G. Levy, S. Zhdanovich, A. K. Mills, D. J. Jones, J. L. Mi, B. B. Iversen, Ph. Hofmann, and A. Damascelli, *arXiv:2105.09320*.
- [59] Y. S. Hor, A. J. Williams, J. G. Checkelsky, P. Roushan, J. Seo, Q. Xu, H. W. Zandbergen, A. Yazdani, N. P. Ong, and R. J. Cava, *Phys. Rev. Lett.* **104**, 057001 (2010).
- [60] M. Kheirkhah, Z. Yan, Y. Nagai, and F. Marsiglio, *Phys. Rev. Lett.* **125**, 017001 (2020).
- [61] N. Goldman, J. C. Budich, and P. Zoller, *Nat. Phys.* **12**, 639 (2016).